Variability in vegetation indices as a function of unmanned aerial vehicle flight altitudes and other factors for crop monitoring applications

Milton Valencia-Ortiz[1], Rebecca J. McGee[2], Arron H. Carter[3], Sindhuja Sankaran[1*]

(1. Department of Biological System Engineering, Washington State University, Pullman, WA 99164, USA;
2. Grain Legume Genetics and Physiology Research Unit, US Department of Agriculture-Agricultural Research Service (USDA-ARS), Pullman, WA 99164, USA;
3. Department of Crop and Soil Sciences, Washington State University, Pullman, WA 99164, USA)

Abstract: Unmanned aerial vehicles (UAV) integrated with multispectral sensors have been widely used for phenotyping in plant breeding programs and other agricultural applications. However, the effect of flight altitude, radiometric correction, and stitching software on the values and variability of the vegetation indices (VI) remain unexplored. Therefore, this study aims to investigate the effect of these factors to better understand their impact on VI variability. In this study, we used wheat and pea trials to evaluate the effect of using different reference reflectance panels for the radiometric correction as a function of flight altitude on commonly used vegetation indices. Pea and wheat data were collected at the initial ripening or flowering stages, respectively. In both trials, single multispectral images were collected at 25 m, 35 m, 45 m, 55 m, 65 m, and 75 m flying altitudes. In addition, UAV was used to collect multispectral images at 25 m, 45 m, and 75 m flying altitude and stitched with multiple photogrammetry software (DroneDeploy, ImageBreed, Agisoft, and Pix4D). For radiometric correction, four Lambertian reference panels were used (10%, 18%, 50%, and 99%). The main results indicated that panels with reflectance of 10% and 20% were suitable for radiometric corrections, since the digital number from these panels did not saturate in most cases. In addition, the correction using the 18% reflectance panel demonstrated consistent reflectance response across flight altitudes. Nevertheless, differences in responses were observed as a function of the flight altitudes after orthomosaic generation, especially with DroneDeploy, ImageBreed, and Pix4D. Vegetation index values, such as normalized difference vegetation index, were highly affected by photogrammetry software. These findings highlight the importance of optimizing UAV-multispectral flight altitudes and radiometric correction approaches to improve the accuracy and stability of vegetation indices in UAV-based crop monitoring, contributing to more precise data for decision-making in plant breeding and precision agriculture applications.

Key words: radiometric correction, multispectral, photogrammetry software, pea, wheat

Citation: Valencia-Ortiz, M., R. J. McGee, A. H. Carter, and S. Sankaran. 2025. Variability in vegetation indices as a function of unmanned aerial vehicle flight altitudes and other factors during crop monitoring applications. Agricultural Engineering International: CIGR Journal, 27(2): 268-284.

1 Introduction

Remote sensing technologies and tools have augmented the resources available to plant breeders and agronomists for crop assessment (Herzig et al.,

Received date: 2024-02-26 **Accepted date:** 2024-11-17

***Corresponding author: Sindhuja Sankaran,** Department of Crop and Soil Sciences, Washington State University, Pullman, WA 99164, USA. Email: s.sankaran@wsu.edu.

2021; Shakoor et al., 2019; Weiss et al., 2020). One of the common tools used for crop monitoring is multispectral sensors integrated into unmanned aerial vehicles (UAV). Vegetation indices can be extracted from the resulting images (Banerjee et al., 2021; Sankaran et al., 2015; Zhang et al., 2021) providing a non-invasive and high-throughput data acquisition capabilities (Chivasa et al., 2021; Tattaris et al., 2016) useful for trait prediction (Fei et al., 2023; Hassan et al., 2019; Herzig et al., 2021) and classification (Barreto et al., 2023; Jarolmasjed et al., 2019). Despite the widespread use of UAV-based multispectral imagery applications, ensuring consistent and comparable vegetation indices (VIs) remains challenging. Factors such as flight altitude, radiometric correction, and photogrammetric software can introduce variability in vegetation indices, which challenges their reliability for decision-making.

Collecting accurate at-surface reflectance data can be difficult for UAV-multispectral systems. Factors such as atmospheric, solar, and topographic effects can impact the accuracy of vegetation indices (Schowengerdt, 1997). Correction for sensor black-level, sensitivity, gain, exposure, and vignetting effects associated with the sensor itself are also important considerations (Micasense, 2024). For example, it is well documented that the solar zenith angle impact significantly affects the VIs values (Galvao et al., 2004; Middleton, 1991; Valencia-Ortiz et al., 2021). Therefore, radiometric correction is crucial procedure, as it involves converting each pixel represented as a digital number (DN) into reflectance (Campbell and Wynne, 2011). Without a proper radiometric correction, VIs may not capture the actual crop conditions, thus limiting its utility.

In general, absolute radiometric correction approaches are commonly used to correct the multispectral imagery acquired from UAVs, which range from complex models such as the atmospheric radiative transfer models (RTM), which aims to correct for atmospheric effects (Vermote and Roger, 1996) to simple models such as the empirical line calibration (ELC). However, for practical applications, RTM is less attractive due to the difficulty in estimating complex parameters such as leaf biochemical properties, reflectance distribution, leaf transmittance, atmospheric properties, and canopy structure that can affect its accuracy (Kuusk and Nilson, 2000; Smith and Milton, 1999; Wierzbicki et al., 2018). Therefore, the ELC approach is often used due to its ease of implementation and practicality.

The ELC uses single or multiple calibrated lambertian reference panels (LRP) for UAV based multispectral imaging applications. Each panel provides known reflectance values across wavelengths that allow the establishment of a relationship between the DN and the reflectance. There are two methods to implement LRP based radiometric corrections. Firstly, images of an individual LRP at approximately one meter of altitude are collected before or after UAV image acquisitions. This method involves the straightforward technique for correction using ELC approach, which postulates that surfaces with zero reflectance will yield zero radiance and there is a linear association between radiance and reflectance (Naito et al., 2017; Smith and Milton, 1999). Also, it is a part of the protocols implemented in photogrammetric software such as Pix4D, Agisoft (Fawcett et al., 2020), and ImageBreed. The second method to correct images is to place the LRP on the field within the area of interest to ensure that images of the UAV mission will cover it. However, neither method accounts for atmospheric corrections (Smith and Milton, 1999).

The ELC can be implemented with multiple reflectance panels (Smith and Milton, 1999) to address the atmospheric effects. This approach allows the user to construct a linear regression between surface reflectance across multiple reflectance panels and DN (radiance at sensor) for each wavelength. Here, a linear equation is used to predict the reflectance of target pixels based on the radiance (Kruse et al., 1990; Smith and Milton, 1999; Xu et al., 2019). However, the ELC can sometimes lead to reflectance values being negative or greater than one (Kizel et al., 2017) and saturated DN data are

observed with high reflectance levels (Deng et al., 2018; Wang and Myint, 2015). Recently, algorithms have been developed to include absolute correction in UAV based multispectral images without the use of LRP. For example, Schneider-Zapp et al. (2019) extracted a hemispheric-directional reflectance factor based on downwelling irradiance sensor, when using a multispectral camera (Parrot Sequoia) using Pix4D photogrammetric software. In this study, we investigated the effect ELC approaches on radiometric correction of multispectral images using calibrated LRPs.

The impact of flight altitudes and radiometric correction across different photogrammetric software on UAV-multispectral derived features has not been studied. With a range of software used in the field, we believe that variability in the data may limit the comparison between studies. For these reasons, we aim to provide insights into the stability of DN, reflectance, and VIs, which are crucial for accurate crop monitoring. In this study, we assess the stability of DN, reflectance, and vegetation indices extracted from multispectral images radio metrically corrected, stitched, and orthorectified using different approaches based on the analysis of variance and relationship with grain yield. The specific objectives were: (1) Evaluate the impact of six flight altitudes (25 – 75 m) on the digital number and reflectance of two crop variants (varieties or breeding lines) using a single multispectral image; (2) Assess the stability of DN and reflectance of two crop variants after radiometric corrections using three LRP with different levels of reflectance, three flight altitude, and four photogrammetric software; and (3) Assess the stability of the vegetation indices across three flight altitudes and stability across photogrammetric software. These findings will be critical for utilizing such data in agricultural applications, enabling more precise crop monitoring.

2 Materials and methods

2.1 Study locations, planting details and grain yield

Winter pea (*Pisum sativum* L.) and soft white winter wheat (*Triticum aestivum* L.) plant breeding trails were chosen to assess the consistency of DN, reflectance, and vegetation indices across different altitudes and photogrammetry software. The pea trail was located at Dayton (Location 1), Washington, United States (46°29'00.7"N 117°57'35.5"W) and wheat trail was located at Pullman (Location 2), Washington, United States (46°41'44.5"N 117°08'18.7"W). From these trails, three remote sensing datasets were constructed. The first dataset was used to check the impact of UAV flight altitude and reflectance using single images (Figure 1). The second dataset was used to evaluate an ELC with different reflectance levels at three UAV flight altitudes on two genotypes of each crop (Figure 1). The third dataset was used to assess the vegetation indices sensitivity and relationship with grain yield across UAV flight altitudes and photogrammetric software.

The first dataset comprised two plots that were spatially close to each other in the winter pea trial (crop variety ‘Goldenwood’ and breeding line PS07300124) and two adjacent plots in the winter wheat trial (crops varieties ‘Stephens’ and ‘Rosalyn’) (Figure 1). For the second dataset, the same genotypes were used, but this time three plots per genotype were analysed. Rosalyn and PS07300124W were spatially distributed, whereas Stephens and Goldenwood were present in the border plots (Figure 1). The third dataset involved 10 pea breeding lines arranged in a randomized complete block design with three replications and 30 wheat breeding lines arranged in a randomized complete block design with two replications (Figure 1). The pea plot size was 1.2 m × 4 m; the wheat plot size was 1.0 m × 3.0 m. In all trials, standard agronomic procedures were employed to manage the fertilization, pests, and weeds during the entire experimental period. The pea trial was planted on 5 October 2021 and harvested on 22 July 2022, while the wheat trial was planted on October 25, 2021, and harvested on August 17, 2022. The primary trait used as a ground reference in the wheat trial was

grain yield (GY), and the trial was harvested using a small plot combine. Pea grain yield data was excluded from the analysis due to the significant canopy overlap leading to inconsistent yield data.

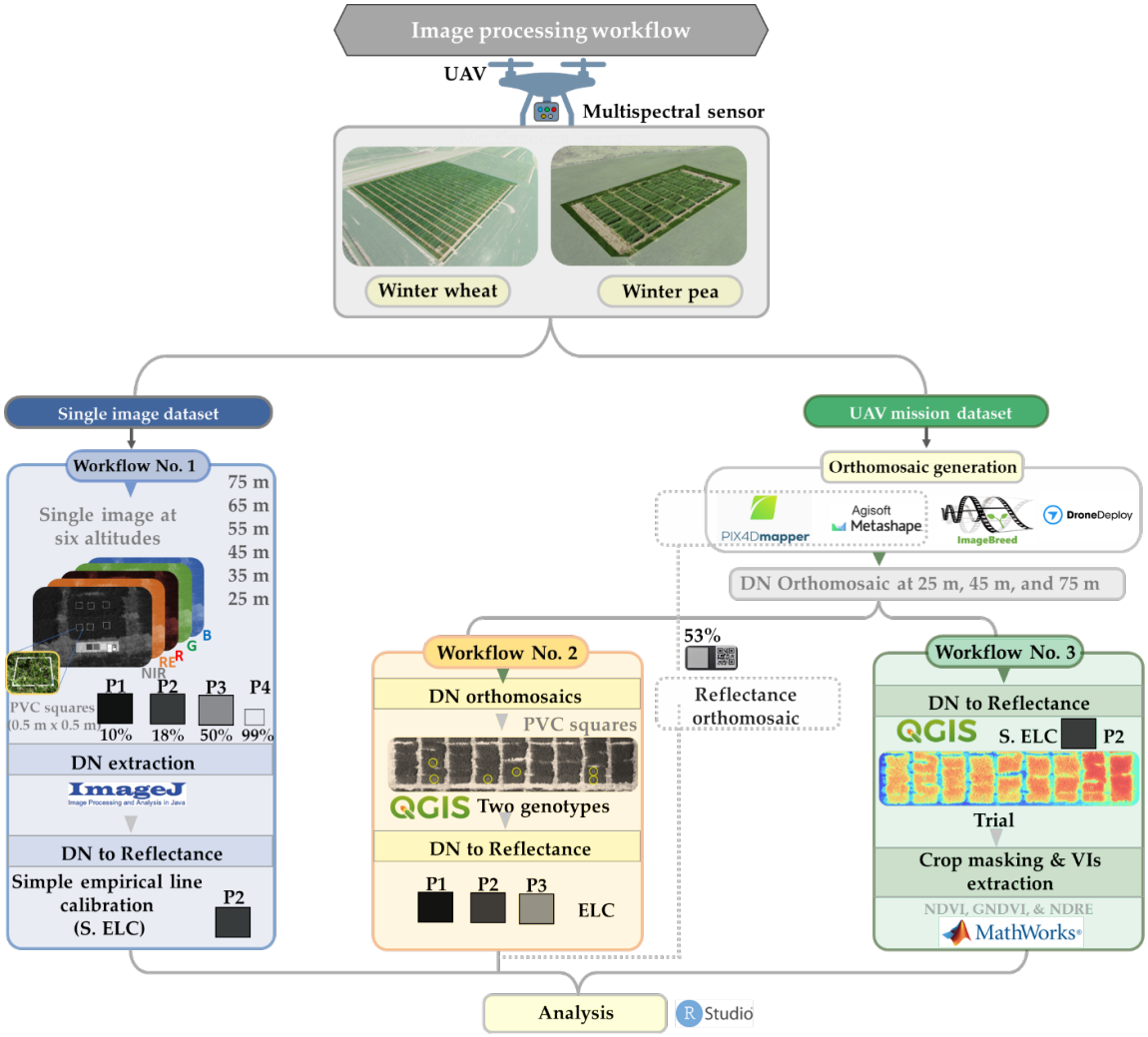

Figure 1 Image processing workflow across multispectral dataset, UAV flight altitudes, photogrammetric software, and crop type

2.2 UAV multispectral data collection

Figure 1 illustrates the UAV multispectral data acquisition process. In this study, a 1.2-megapixel multispectral sensor (RedEdge, Micasense Inc., Seattle, Washington, USA) was integrated with a UAV quadcopter (AgBotTM, ATI/Aerial Technology International, Oregon City, Oregon, USA). This sensor contains blue, green, red, red edge (RE), and near-infrared (NIR) filters with center and bandwidth of 475 ± 32 nm, 560 ± 27 nm, 668 ± 14 nm, 717 ± 12 nm, and 842 ± 57 nm, respectively. Radiometric resolution of 16-bits corresponded to a DN range between 0 and 65,535. During workflow 1, three PVC squares (0.5 m × 0.5 m) were made and used to delimit the regions of interest of plots that were placed on top of the crop canopy; the data within the delimited regions were used to extract vegetation reflectance for further analysis. Four LRPs were placed at one side of the plot (P1 = 10% (PFT-10-05M-RT-TC), P2 = 18% (PFT-18-05M-RT-TC), P3 = 50% (PFT-50-05M-RT-TC), P4 = 99% (SRS-99–120) (Labsphere®, North Sutton, New Hampshire, USA). Finally, the UAV was operated manually to collect single-shot images at 25, 35, 45, 55, 65, and 75 m above ground level using a remote control with a spatial resolution of 1.74 cm pixel^{-1}, 2.43 cm pixel^{-1}, 3.13 cm pixel^{-1}, 3.82 cm pixel^{-1}, 4.51 cm pixel^{-1}, and 5.21 cm pixel^{-1}, respectively (Figure 1).

During workflows 2 and 3, the PVC squares were rearranged, placing one PVC square per plot per replicate for each genotype with a total of three replications per genotype (Figure 1). The same panels (P1, P2, P3 and P4) were also placed on one side of the field. In addition, a fifth panel (P5 = 53%, RP04-

1949243-OB, Micasense Inc., Seattle, WA, USA) was used to collect one image of the panel at 1 m flight altitude before deploying the UAV mission (this panel was used only for Pix4D and Agisoft metashape radiometric correction). Three missions using the QGroundControl station (qgroundcontrol.com) with three flight altitudes (25 m, 45 m, and 75 m) were programmed with an overlap of 80% horizontal and 70% vertical, a speed of 3.0 m s^{-1}, and a camera angle of 90º. The spatial resolution was 1.74 cm $pixel^{-1}$, 3.13 cm $pixel^{-1}$, and 5.21 cm $pixel^{-1}$ at 25 m, 45 m, and 75 m, respectively (Figure 1). In both data collection sequences, single image and UAV grid mission, the sensor was set to automatic gain and exposure. Table 1 describes the environmental conditions during the UAV data acquisition at both trial locations.

Table 1 Environment conditions during UAV data acquisition.

Location	Collection time	Solar radiation ($W.m^{-1}$)	Temperature (ºC)	Relative humidity (%)
Spillman	13:00:00	925	19.4	42.9
Dayton	15:00:00	830	19.9	49.6

2.3 Images processing: single images

The single multispectral images acquired at 25, 35, 45, 55, 65, and 75 m flight altitudes were processed in ImageJ (V1.53; NIH, Bethesda, MD, USA) to extract the digital number for each wavelength and crop trial. Canopy reflectance (Rc) was estimated using the simple empirical line calibration method (Smith and Milton, 1999) with a reflectance panel of 18% (based on observed saturation in other reflectance panels) (Figure 1) as follows:

$$Rc = \frac{DNc}{DNp} \quad (1)$$

Where, *DNc*, *DNp*, and *Rc* represent the digital number of the crop, the digital number of the reference panel, and the reflectance factor of reference panel at specific wavelength.

2.4 Images processing: images from the UAV missions

Datasets collected from UAV multispectral system at 25 m, 45 m, and 75 m were processed with Pix4Dmapper (Pix4D S.A. Switzerland, v4.4.12), Agisoft Metashape (Agisoft LLC., St. Petersburg, Russia, v1.8.3), online cloud server DroneDeploy (DroneDeploy, CA, USA), and ImageBreed version 10.1 (Morales et al., 2020) to generate DN orthomosaic images for each flight at each crop trial. In Pix4D, the initial image processing step involved uploading the raw images, followed by point cloud generation to create a digital surface model and the DN orthomosaic imagery (orthomosaic image from mosaic folder was used in this study). In Agisoft, the raw images were also uploaded, and the subsequent steps involved alignment and optimized alignment. Subsequently, the point cloud was used to generate a digital elevation model and construct the DN orthomosaic imagery. The cloud-based computing process for DroneDeploy did not provide specific options associated with the image processing steps. In the case of ImageBreed, the cloud-based computing image processing entailed uploading images and providing additional information such as field trial details, image acquisition date, image resolution, and sensor type.

The DN orthomosaic images from different photogrammetric software were used for radiometric correction. Next, QGIS (version 3.30.1) was used to extract DN values of square PVC regions across software, flight altitudes, and crop type. QGIS was used for canopy masking, and wavelength-specific reflectance extraction was performed using the square regions (0.5 m × 0.5 m) from the two different genotypes of each crop. Radiometric correction was applied using the ELC method in RStudio using single panel reflectance data and panel combination data. For combined panels, the following linear equation was used:

$$R = b + DN \times m \quad (2)$$

where, *R* is the estimated reflectance, *DN* is the digital number, and *b* and *m* are the regression coefficients (intercept and slope, respectively). Pix4Dmapper and Agisoft Metashape were used to

generate reflectance orthomosaics, from the Micasense reflectance panel (53%) images collected at 1 m of altitude (Figure 1), that were then used to compare the ELC approaches in this study. It's worth noting that the radiometric correction algorithms used in this software are black-box procedures. However, the single reflectance panel is only a part of the calibration procedure that also involves other factors such as sensor settings, sensor properties, and scene conditions (Pix4D, 2024); however, in scene conditions, the downwelling light sensor option was turned off in both software.

2.5 Images processing: vegetation indices extraction

Pix4D, DroneDeploy, Agisoft metashape, and ImageBreed software were used to generate DN orthomosaics across 25 m, 45 m, and 75 m altitudes and crop types. QGIS was used to apply simple ELC using an 18% reflectance panel. Matlab (2018b; MathWorks Inc., Natick, MA, USA) (Zhang et al., 2021) was used to create a mask of the crop canopy and extract three typical normalized vegetation indices (VIs) per plot using green (G), red (R), rededge (RE), and near-infrared (NIR) wavelengths: Normalized Difference Vegetation Index/NDVI (Rouse et al., 1974), Green Normalized Difference Vegetation Index/GNDVI (Gitelson et al., 1996), and Normalized Difference Red Edge Index/NDRE (Gitelson and Merzlyak, 1994) (Figure 1). These VIs are widely used in plant breeding programs due to their association with yield and related agronomic traits at reproductive and grain development stages (Lozada et al., 2020; Shafiee et al., 2021; Valencia-Ortiz et al., 2021; Zhang et al., 2021).

2.6 Statistical analysis

RStudio software (Version 4.2.3, 2023, Boston, MA) was used to analyse the output data. The ggplot2 package was used for descriptive plot visualization as well as the inference analysis. Outliers were removed using the interquartile range method (Handakumbura et al., 2019) during digital trait analysis and data were normalized using the Box-Cox function (MASS package). Analysis of variance and post-hoc Tukey's test analysis (R function, lme4, and multcomp package) were used to evaluate the digital trait sensitivity across flight altitudes and photogrammetry software. Finally, Pearson's correlation (R function) was used to evaluate the association of the digital trait with wheat grain yield.

3 Results and discussion

3.1 Digital number and reflectance across flight altitudes using single image data

The quality of an image relies heavily on camera exposure, which is determined by the shutter speed, aperture, and ISO. When these parameters are not adequately balanced, pixel saturation can occur. Pixel saturation happens when the incoming light at a pixel reaches its maximum value (Zhang and Brainard, 2004). For Micasense multispectral sensors, it is recommended to leave the ISO and exposure settings on automatic mode as they are optimized across image captures and wavelengths (Micasense, 2022). However, in this study, the saturation of the rescaled DN (0 to 1) response was observed at specific wavelengths with specific reflectance panels using a single image dataset. The P4 showed saturation across wavelengths from data collected at Pullman and Dayton locations and at six flight altitudes (Figure 2a). Wang and Myint (2015) found a similar saturation in the red wavelength using a reflectance panel of 94%. A similar observation was made using a P3 reflectance panel, except for the near-infrared wavelength did not saturate (Figure 2a). Deng et al. (2018) reported that DN saturation only affected a part of the visible region of the multispectral camera (Sequoia-PIX sensor) at 50 m of altitude with 40% and 60% reflectance panels.

P1 and P2 did not show saturation, except for P2 at the blue wavelength beyond 45 m flight altitude in Dayton and 75 m flight altitude in Pullman; however, blue, green, red, and red edge wavelength exceeded the DN intensity compared to NIR spectral band (Figure 2a). This limitation was also reported in the visible region of the multispectral data using reference panels ranging from 22% to 63%

(Chakhvashvili et al., 2021). Generally, higher altitudes were associated with higher DN values (Figure 2a). A similar trend was also reported by Guo et al. (2019). These results indicate that some wavelengths, such as RE and NIR, are less sensitive to saturation, and the high flight altitude can lead to saturation responses across wavelengths. This finding holds significant value in determining the suitable panels for further radiometric correction. Since P2 did not saturate in visible and near-infrared regions in most cases, we used the 18% reflectance panel to apply radiometric correction from the panel at a specific flight altitude to the individual crop images acquired at the same flight altitude. Upon correction, only minor variations were observed in crop reflectance values across altitudes (Figure 2b). Similarly, the crop line canopy reflectance response showed a typical pattern of plant reflectance across six flight altitudes. Furthermore, the green reflectance was found to be higher in pea lines than in wheat lines (Figure 3). Interestingly, the green reflection in wheat lines was slightly higher at an altitude of 25 m than at higher altitudes.

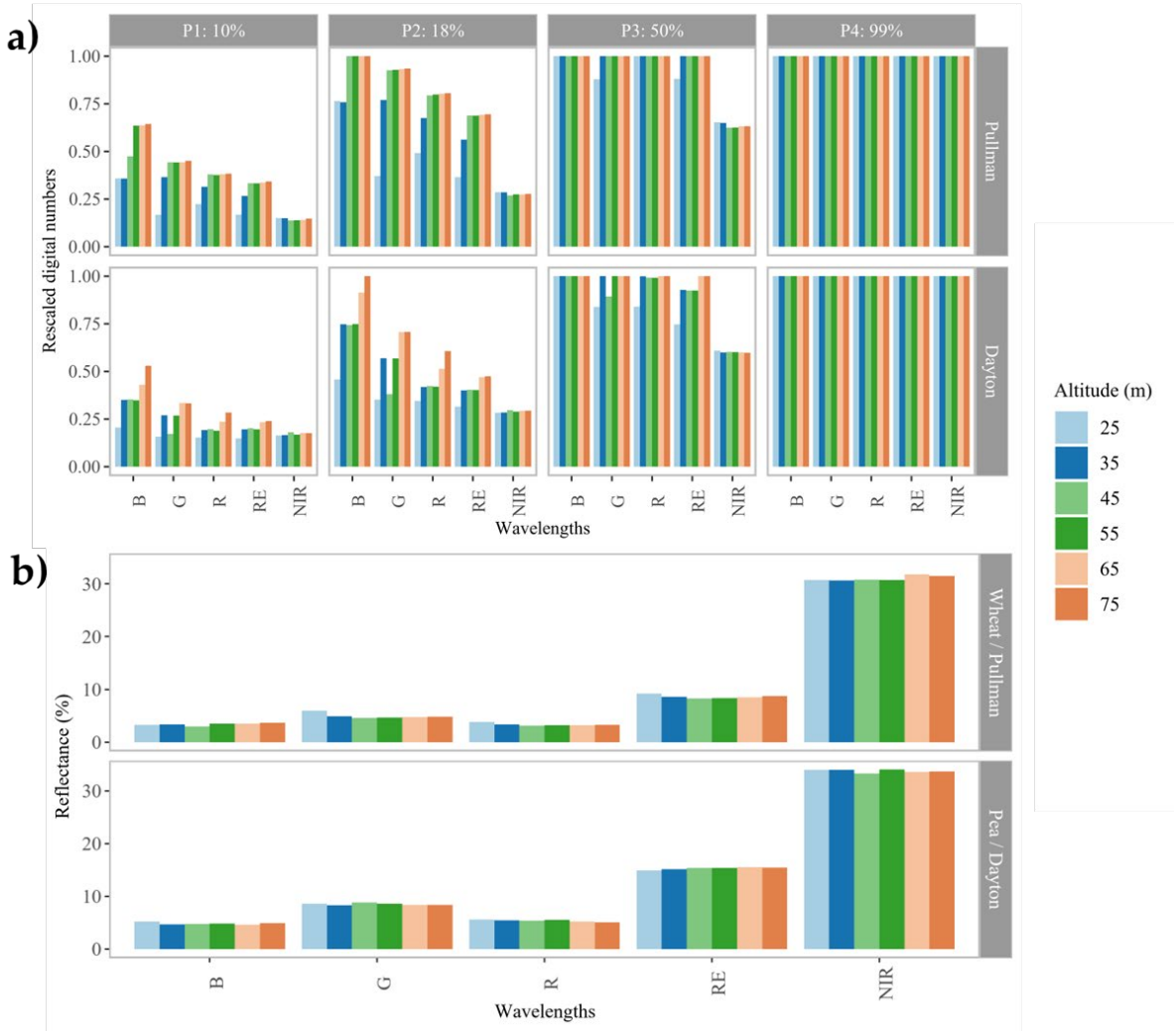

(a) Spectral response as digital numbers of single multispectral image across reflectance panels and flight altitudes (b) Spectral reflectance response of single multispectral image from 18% panel across flight altitudes

Figure 2 Digital number and spectral reflectance data

The digital responses of multispectral images can be influenced by the algorithms employed in photogrammetry software under different UAV flight altitudes. At each location (Pullman and Dayton), similar digital patterns on reference panels (P1, P2, P3, and P4) across wavelengths and photogrammetry software were observed (Supplementary Materials, Figure S1). Similar to the single image data, the wavelengths in the high reflectance panel (P3 and P4) often displayed a DN saturation. For P1 and P2, the

photogrammetry software also showed high DN responses as flight altitude increased that led to saturation problems; however, the saturation changed as a function of photogrammetry software and location. For example, at the Pullman location using P2, both ImageBreed and Pix4D showed saturation in the blue and green wavelength, whereas at Dayton, only the blue wavelength exhibited saturation. Additionally, Drone Deploy displayed saturation in the red wavelength at Dayton, whereas at Pullman, both the red and green wavelengths were close to saturation (Supplementary Materials, Figure S1). These results suggest that panel DN response is influenced by flight altitude, photogrammetry software, and environment. Togeirode Alckmin et al. (2022) also found problems with DN saturation using high reflectance panels, and therefore, exclusively utilized dark panels for ELC. This observation aligns with the findings reported by Cao et al. (2019) where two panels of low reflectance were selected for reflectance calibration; also, Olsson et al. (2021) recommend using reflectance panels lower than 20% to prevent DN saturation and obtain a more reliable value to use in empirical line calibration. Based on these findings, we can conclude that panels with low reflectance effectively prevent saturation, and singly or in combination are suitable to convert DN into reflectance.

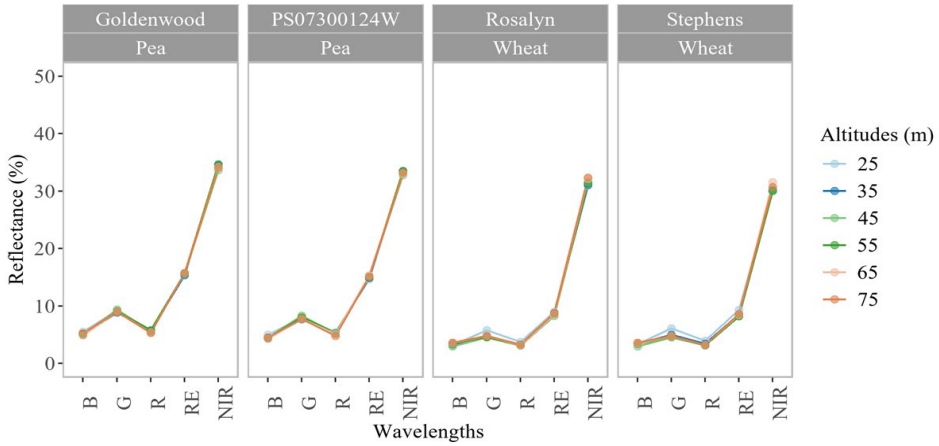

Figure 3 Multispectral reflectance pattern across flight altitudes using a single image

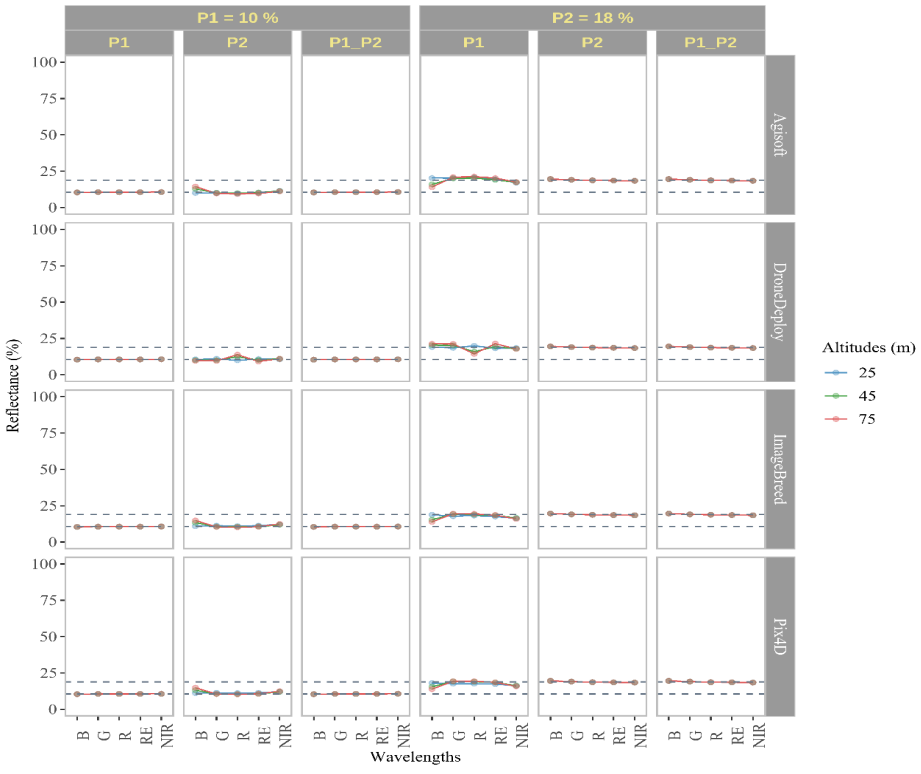

Figure 4 Reflectance panel response after radiometric correction

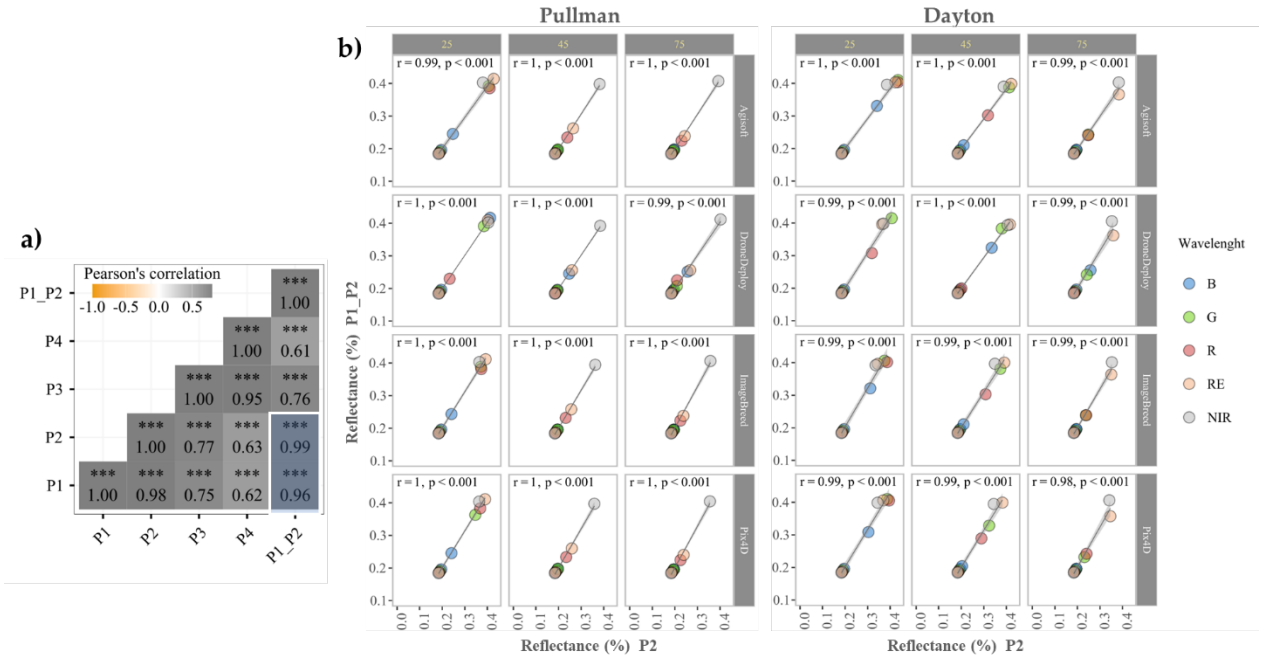

(a) Correlation coefficient between different reflectance panels (b) Correlation and linear trend of P2 (18%) and combined panels (P1:10% and P2:18%)

Figure 5 Pearson's correlation analysis

3.3 Effect of radiometric correction across flight altitudes and photogrammetric software

Based on previous results P1, P2, and the combination (P1 and P2) were used for radiometric correction on orthomosaics generated from different photogrammetric software and flight altitudes. When P1 and P2 were used either independently or in combination, the reflectance responses were satisfactory (Figure 4). There was a strong and statistically significant correlation between P1 and P1_P2 (r = 0.96, p <0.001, Figure 5a), with the highest correlation between single panel (P2) and the combined panels (P1_P2) (r = 0.99, p<0.001, Figure 5a). This association was examined across flight altitudes and photogrammetric software at Pullman and Dayton locations (Figure 5b) and the correlation was significant at all altitudes and with all software.

The radiometric correction using P2 was also compared with the reference panel at 1 m (P5). This comparison found a strong and significant correlation with Agisoft and Pix4D across altitudes (ranging from 0.93 to 0.99, with a p= 0.001, Supplementary Materials, Figure S2). Additionally, crop reflectance (radiometrically corrected with P2) was compared with the rescaled DN response. In addition to converting DN into physical data for data comparisons (Campbell and Wynne, 2011) and quantitative analysis (Smith and Milton, 1999), radiometric correction also plays a role in adjusting the reflectance ratios across different wavelengths that improves the reflectance estimation. For example, the RGB spectrum ratios were adjusted after radiometric correction (Supplementary Materials, Figure S3).

3.4 Analysis of variance (ANOVA) of crop traits across flight altitudes and photogrammetric software

After the generation of the orthomosaic and the implementation of radiometric calibration using an 18% panel, the reflectance response exhibited variations across different flight altitudes (Figure 6). For example, notable variations were observed in the green, RE, NIR across the flight altitudes. However, Agisoft demonstrated lower variation and more consistent reflectance values across flight altitudes compared to Pix4D, ImageBreed, and DroneDeploy. The sensitivity analysis of VIs (NDVI, GNDVI, and NDRE) that involves green, red, RE, and NIR wavelengths indicated a highly significant impact of UAV flight altitude (Figure 6). This result is unlike

those reported in Hernández-López et al. (2012) where no atmospheric effect at GSD of 10 cm was observed across different surfaces including grass. Similarly, Rasmussen et al. (2016) also reported no effect of flight altitudes between 1 m to 100 m on VIs from winter barley (*Horedum vulgare* L.).

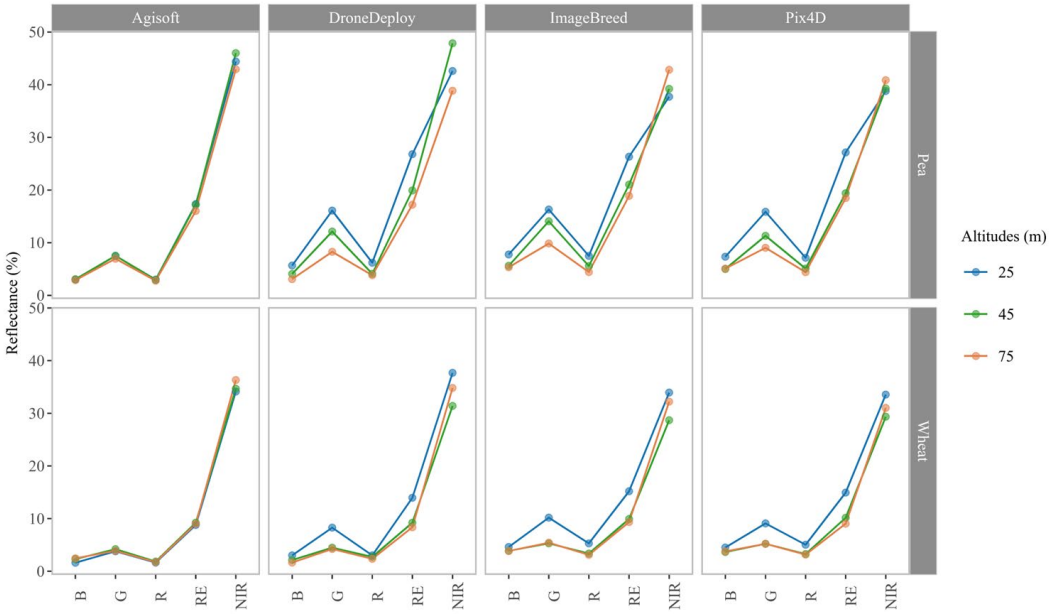

Figure 6 Crop reflectance response across flight altitudes, photogrammetric software and crop type. Values represent the mean of 30 and 60 plots from pea and wheat trials, respectively

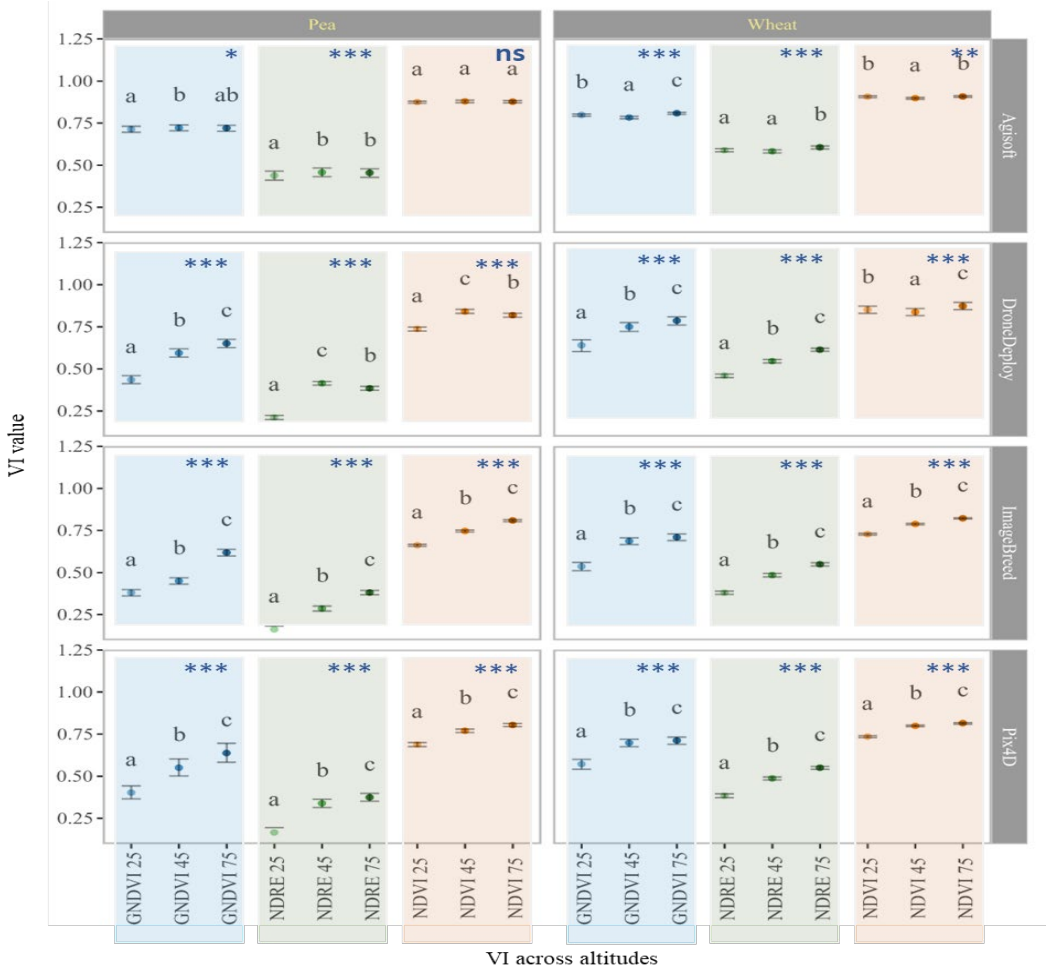

Figure 7 Analysis of variance of vegetation indices across flight altitudes. Asterisks indicate the level of significance (*p< 0.5, **p< 0.01, ***p< 0.0001)

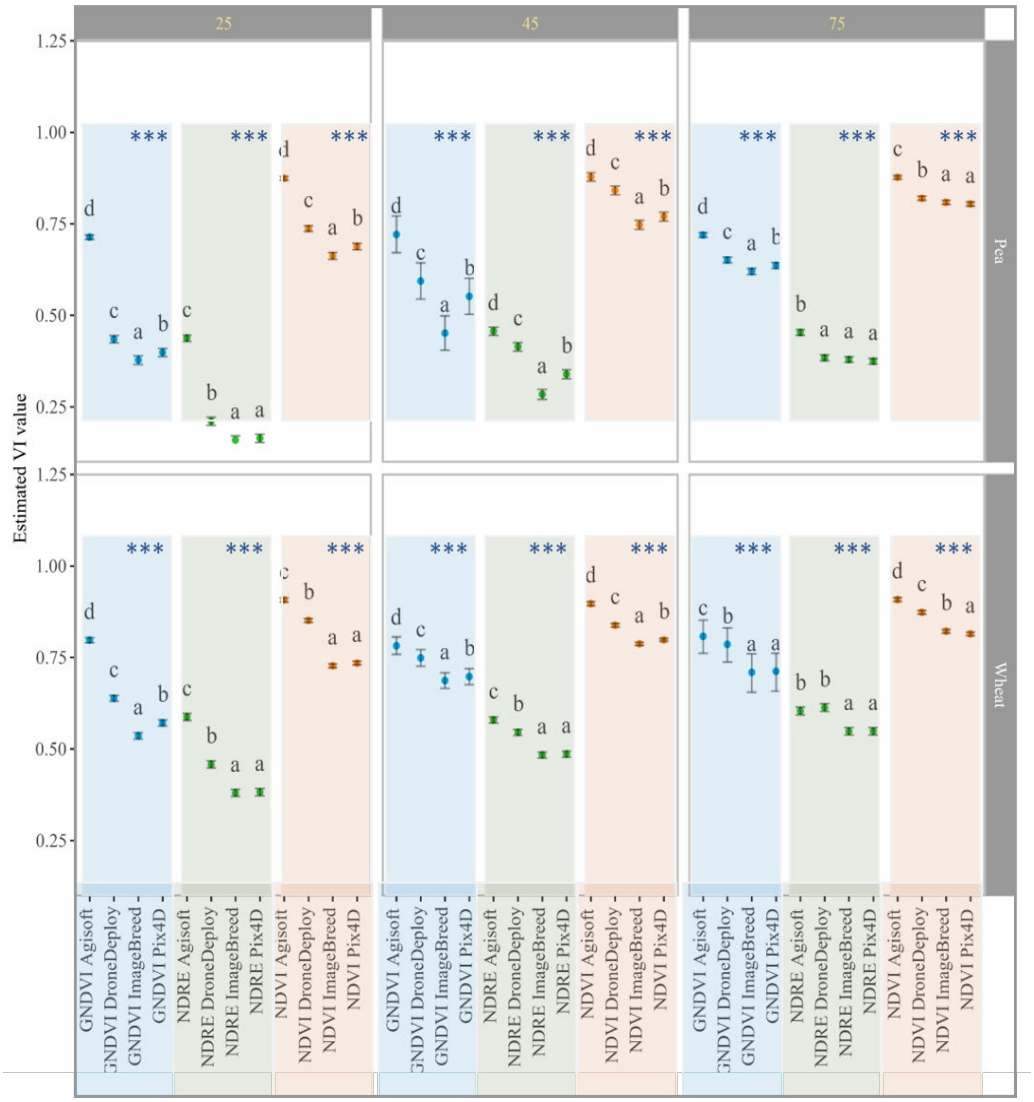

Figure 8 Analysis of variance of vegetation indices and photogrammetric software. Asterisks indicate the level of significance (***p< 0.0001)

For Pix4D, ImageBreed, and DroneDeploy, the posthoc analysis revealed a significant increase in VI values as altitude increased. Jiang et al. (2020) also mentioned that the flight altitude affected the NDVI of paddy rice (*Oryza sativa* L.), however, in their study, the mean NDVI values increased as flight altitude decreased. Stow et al. (2019) reported no conclusive effect of flight altitude; however, in their study, the NDVI values from grasses and moss vegetation showed variation at the first 25 m, similar to this work. In the case of Agisoft, the VIs values remained relatively stable across altitudes for both trials (Figure 7).

The photogrammetric software significantly affected the VIs responses across flight altitudes (p<0.0001). Among the software, Agisoft exhibited the highest VI values across altitudes and crop types, closely followed by DroneDeploy. This result is different from those reported by Kharuf-Gutierrez et al. (2018), where Agisoft yielded lower NDVI values in sugarcane (*Saccharum officinarum* L.) than Pix4D, unlike our results. Taddia et al. (2020) indicated a small variation in the seaweed NDVI frequency, distribution between Agisoft and Pix4D data, whereas Boon and Tesfamichael (2017) reported similar NDVI responses. On the other hand, ImageBreed and Pix4D produced lower VI values that were relatively consistent across most altitudes and crop types (Figure 8). Rasmussen et al. (2016) also reported significant variation in VIs as function of stitching software (Microsoft ICE and Pix4D). The variation in VIs may be a result of different photogrammetry

approaches used during image stitching and orthorectification. More details on Pix4D's orthorectification process can be found in Strecha et al. (2008).

The relationship between extracted VI data and yield data was also assessed in wheat trials. In general, Pix4D displayed the highest positive linear relationship between VIs and grain yield across different flight altitudes, followed by ImageBreed. However, it is worth noting that ImageBreed did not show a significant correlation at 25 m with the GNDVI and NDRE indices (Figure 9). In Avtar et al. (2020), 60 and 80 m flight altitude data showed better relationship with the oil palm (*Elaeis guineensis* Jacq.) biophysical parameters. In the current study, the 45 m and 75 m data were better correlated with seed yield than 25 m, especially with Pix4D software (Figure 9). In addition, there was comparable correlation when using either an 18% Labsphere panel or a 53% Misasense panel for radiometric correction with either Pix4D or Agisoft software (Figure 9).

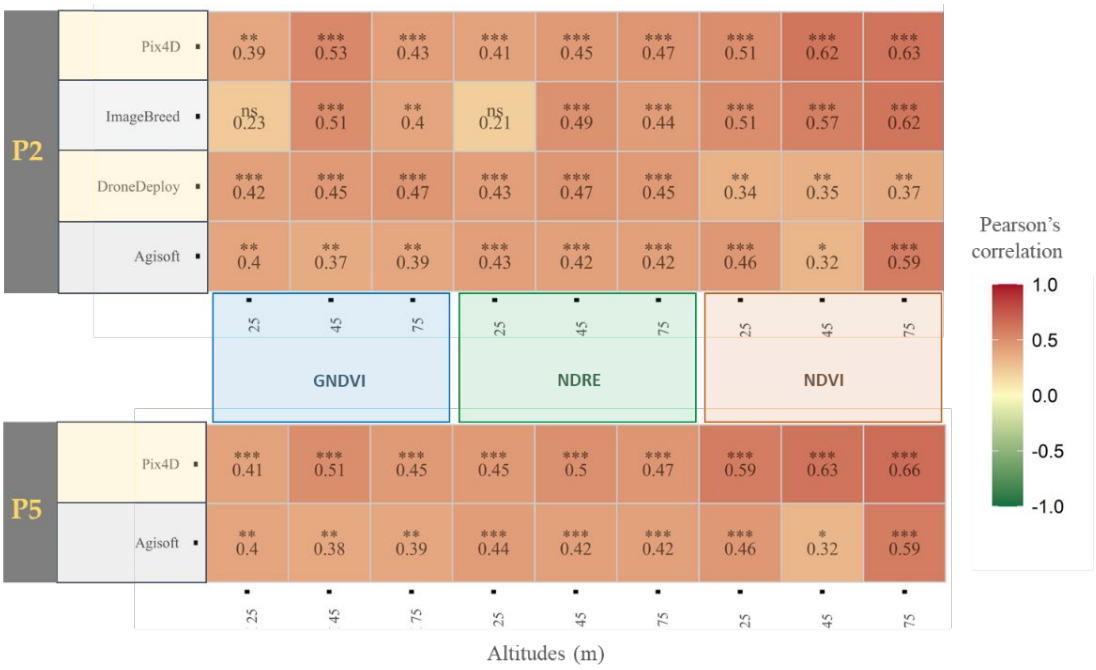

Figure 9 Pearson correlation coefficient between wheat grain yield and vegetation using P2: 18% and P5: 53% panels. Asterisks indicate the level of significance (*p< 0.5, **p< 0.01, ***p< 0.0001)

4 Conclusions

In this study, we found that radiometric correction analysis using two reflectance panels (10% and 18%), alone or in combination, exhibited acceptable and consistent reflectance values for green, red, and red-edge wavelengths without encountering saturation issues. Notably, strong linear associations were observed between the 18% panel and the Micasense panel (53%) when using Pix4D and Agisoft software. Furthermore, a sensitivity analysis revealed that the UAV flight altitudes across different software and crop types impacted the vegetation indices due to atmospheric and sensor effects. Generally, higher altitudes led to elevated VI values; however, this effect was minimal for VIs extracted from Agisoft. Additionally, the sensitivity analysis underscored the significant impact of each VI within the various software platforms. This information is of utmost importance for characterizing UAV multispectral data, as it involves pre-processing images and analysis of VIs to predict agronomic traits.

Supplementary Materials: Figure S1: Rescaled digital number response from four reflectance panels (10%, 18%, 50%, and 99%), two locations (Pullman and Dayton), and four photogrammetric software (Agisoft, DroneDeploy, ImageBreed, and Pix4D); Figure S2: Crop reflectance correlation between panel of 18% (P2) and Micasense panel of 53% (P5) across altitudes and two photogrammetric software (Agisoft and Pix4D); Figure S3: Spectral plant reflectance

(radiometrically corrected with P2= 18%) and rescaled digital number across crop type, photogrammetric software, and flight altitudes. For this comparison, DN values were rescaled between 0 to 100.

Acknowledgments

We would like to thank Kingsley Umani and Kyall Hagemeyer for their help during data collection.

Conflicts of Interest

The authors declare no conflict of interest.

Funding

This study was funded by the United States Department of Agriculture (USDA)—National Institute for Food and Agriculture (NIFA) competitive, hatch and multistate projects (accession number 1028108, 7003737, Wheat CAP grant #2022-68013-36439, NC1212), and USDA Agricultural Research Services (ARS) Research Service Agreements (58-2090-2-029, 58-2090-3-031).

References

Avtar, R., S. A. Suab, M. S. Syukur, A. Korom, D. A. Umarhadi, and A. P. Yunus. 2020. Assessing the influence of UAV altitude on extracted biophysical parameters of young oil palm. *Remote Sensing*, 12(18): 3030.

Banerjee, B. P., V. Sharma, G. Spangenberg, and S. Kant. 2021. Machine learning regression analysis for estimation of crop emergence using multispectral UAV imagery. *Remote Sensing*, 13(15): 2918.

Barreto, A., F. R. Ispizua Yamati, M. Varrelmann, S. Paulus, and A. K. Mahlein. 2023. Disease Incidence and Severity of Cercospora Leaf Spot in Sugar Beet Assessed by Multispectral Unmanned Aerial Images and Machine Learning. *Plant Disease*, 107(1): 188-200.

Boon, M. A., and S. Tesfamichael. 2017. Wetland vegetation integrity assessment with low altitude multispectral UAV imagery. In *International Archives of the Photogrammetry, Remote Sensing and Spatial Information Sciences*, 55-62. Bonn, Germany, 4–7 September.

Campbell, J. B., and R. H. Wynne. 2011. *Introduction to Remote Sensing*. 5th ed. New York:The Guilford Press.

Cao, S., B. Danielson, S. Clare, S. Koenig, C. Campos-Vargas, and A. Sanchez-Azofeifa. 2019. Radiometric calibration assessments for UAS-borne multispectral cameras: Laboratory and field protocols. *ISPRS Journal of Photogrammetry and Remote Sensing*, 149: 132-145.

Chakhvashvili, E., B. Siegmann, J. Bendig, and U. Rascher. 2021. Comparison of reflectance calibration workflows for a UAV-mounted multi-camera array system. In *2021 IEEE International Geoscience and Remote Sensing Symposium (IGARSS)*, 8225-8228. Brussels, Belgium, 11-16 July.

Chivasa, W., O. Mutanga, and J. Burgueño. 2021. UAV-based high-throughput phenotyping to increase prediction and selection accuracy in maize varieties under artificial MSV inoculation. *Computers and Electronics in Agriculture*, 184: 106128.

Deng, L., Z. Mao, X. Li, Z. Hu, F. Duan, and Y. Yan. 2018. UAV-based multispectral remote sensing for precision agriculture: A comparison between different cameras. *ISPRS Journal of Photogrammetry and Remote Sensing*, 146: 124-136.

Fawcett, D., C. Panigada, G. Tagliabue, M. Boschetti, M. Celesti, A. Evdokimov, K. Biriukova, R. Colombo, F. Miglietta, U. Rascher, and K. Anderson. 2020. Multi-scale evaluation of drone-based multispectral surface reflectance and vegetation indices in operational conditions. *Remote Sensing*, 12(3): 514.

Fei, S., M. A. Hassan, Y. Xiao, X. Su, Z. Chen, Q. Cheng, F. Duan, R. Chen, and Y. Ma. 2023. UAV-based multi-sensor data fusion and machine learning algorithm for yield prediction in wheat. *Precision Agriculture*, 24(1): 187-212.

Galvao, L. S., F. J. Ponzoni, J. C. N. Epiphanio, B. F. T. Rudorff, and A. R. Formaggio. 2004. Sun and view angle effects on NDVI determination of land cover types in the Brazilian Amazon region with hyperspectral data. *International Journal of Remote Sensing*, 25(10): 1861–1879.

Gitelson, A. A., Y. J. Kaufman, and M. N. Merzlyak. 1996. Use of a green channel in remote sensing of global vegetation from EOS- MODIS. *Remote Sensing of Environment*, 58(3): 289-298.

Gitelson, A., and M. N. Merzlyak. 1994. Spectral Reflectance Changes Associated with Autumn Senescence of *Aesculus hippocastanum* L. and *Acer platanoides* L. Leaves. Spectral Features and Relation to Chlorophyll Estimation. *Journal of Plant Physiology*, 143(3): 286-292.

Guo, Y., J. Senthilnath, W. Wu, X. Zhang, Z. Zeng, and H.

Huang. 2019. Radiometric calibration for multispectral camera of different imaging conditions mounted on a UAV platform. *Sustainability*, 11(4): 978.

Handakumbura, P. P., B. Stanfill, A. Rivas-Ubach, D. Fortin, J. P. Vogel, and C. Jansson. 2019. Metabotyping as a Stopover in Genome-to-Phenome Mapping. *Scientific Reports*, 9(1): 1858.

Hassan, M. A., M. Yang, A. Rasheed, G. Yang, M. Reynolds, X. Xia, Y. Xiao, and Z. He. 2019. A rapid monitoring of NDVI across the wheat growth cycle for grain yield prediction using a multi-spectral UAV platform. *Plant Science*, 282: 95–103.

Hernández-López, D., B. Felipe-García, N. Sánchez, D. González-Aguilera, and J. Gomez-Lahoz. 2012. Testing the radiometric performance of digital photogrammetric images: Vicarious vs. laboratory calibration on the Leica ADS40, a study in Spain. *Photogrammetrie, Fernerkundung, Geoinformation*, 5: 557-571.

Herzig, P., P. Borrmann, U. Knauer, H. C. Klück, D. Kilias, U. Seiffert, K. Pillen, and A. Maurer. 2021. Evaluation of RGB and multispectral unmanned aerial vehicle (UAV) imagery for high-throughput phenotyping and yield prediction in barley breeding. *Remote Sensing*, 13(14): 2670.

Jarolmasjed, S., S. Sankaran, A. Marzougui, S. Kostick, Y. Si, J. J. Quirós Vargas, and K. Evans. 2019. High-throughput phenotyping of fire blight disease symptoms using sensing techniques in apple. *Frontiers in Plant Science*, 10: 576.

Jiang, R., P. Wang, Y. Xu, Z. Zhou, X. Luo, Y. Lan, G. Zhao, A. Sanchez-Azofeifa, and K. Laakso. 2020. Assessing the operation parameters of a low-altitude UAV for the collection of NDVI values over a paddy rice field. *Remote Sensing*, 12(11): 1850.

Kharuf-Gutierrez, S., L. Hernández-Santana, R. Orozco-Morales, O. de la C. Aday Díaz, and I. Delgado Mora. 2018. Análisis de imágenes multiespectrales adquiridas con vehículos aéreos no tripulados. *Ingeniería Electrónica, Automática y Comunicaciones*, 39(2): 79-91.

Kizel, F., L. Bruzzone, and J. A. Benediktsson. 2017. Simultaneous empirical line calibration of multiple spectral images. In *2017 IEEE International Geoscience and Remote Sensing Symposium (IGARSS)*, 4185-4188. Fort Worth, TX, USA, 23- 28 July.

Kruse, F. A., K. S. Kierein-Young, and J. W. Boardman. 1990. Mineral mapping at Cuprite, Nevada with a 63-channel imaging spectrometer. *Photogrammetric Engineering and Remote Sensing*, 56(1): 83.

Kuusk, A., and T. Nilson. 2000. A directional multispectral forest reflectance model. *Remote Sensing of Environment*, 72(2): 244-252.

Lozada, D. N., J. V. Godoy, B. P. Ward, and A. H. Carter. 2020. Genomic prediction and indirect selection for grain yield in US Pacific Northwest winter wheat using spectral reflectance indices from high-throughput phenotyping. *International Journal of Molecular Sciences*, 21(1): 0165.

Micasense. 2024. Radiometric Calibration Model for MicaSense Sensors. Available at: https://support.micasense.com/hc/en-us/articles/115000351194-Radiometric-Calibration-Model-for-MicaSense-Sensors. Accessed 1 February 2024.

Micasense. 2022. Is there a way to manually set gain (ISO) and exposure? Available at: https://support.micasense.com/hc/en-us/articles/215170537-Is-there-a-way-to-manually-set-gain-ISO-and-exposure. Accessed 1 February 2024.

Middleton, E. M. 1991. Solar zenith angle effects on vegetation indices in tallgrass prairie. *Remote Sensing of Environment*, 38(1): 45–62.

Morales, N., N. S. Kaczmar, N. Santantonio, M. A. Gore, L. A. Mueller, and K. R. Robbins. 2020. ImageBreed: Open-access plant breeding web–database for image-based phenotyping. *The Plant Phenome Journal*, 3(1): e2004.

Naito, H., S. Ogawa, M. O. Valencia, H. Mohri, Y. Urano, F. Hosoi, Y. Shimizu, A. L. Chavez, M. Ishitani, M. G. Selvaraj, and K. Omasa. 2017. Estimating rice yield related traits and quantitative trait loci analysis under different nitrogen treatments using a simple tower-based field phenotyping system with modified single-lens reflex cameras. *ISPRS Journal of Photogrammetry and Remote Sensing*, 125: 50–62.

Olsson, P. O., A. Vivekar, K. Adler, V. E. Garcia Millan, A. Koc, M. Alamrani, and L. Eklundh. 2021. Radiometric correction of multispectral UAS images: Evaluating the accuracy of the parrot sequoia camera and sunshine sensor. *Remote Sensing*, 13(4): 577.

Pix4D. 2024. *Radiometric correction - PIX4Dfields*. Available at: https://support.pix4d.com/hc/en-us/articles/ 360022919691-Radiometric-correction-PIX4Dfields. Accessed 1 February 2024.

Rasmussen, J., G. Ntakos, J. Nielsen, J. Svensgaard, R. N. Poulsen, and S. Christensen. 2016. Are vegetation indices derived from consumer-grade cameras mounted on UAVs sufficiently reliable for assessing experimental plots? *European Journal of Agronomy*, 74: 75-92.

Rouse, J. W., R. H. Hass, J. A. Schell, D. W. Deering, and J. C. Harlan. 1974. Monitoring the vernal advancement and retrogradation (green wave effect) of natural vegetation.

Final Report, RSC 1978-4. Texas, USA: Texas A & M University, College Station.

Sankaran, S., L. R. Khot, and A. H. Carter. 2015. Field-based crop phenotyping: Multispectral aerial imaging for evaluation of winter wheat emergence and spring stand. *Computers and Electronics in Agriculture*, 118: 372-379.

Schneider-Zapp, K., M. Cubero-Castan, D. Shi, and C. Strecha. 2019. A new method to determine multi-angular reflectance factor from lightweight multispectral cameras with sky sensor in a target-less workflow applicable to UAV. *Remote Sensing of Environment*, 229: 60-68.

Schowengerdt, R. A. 1997. *Remote Sensing: Models and Methods for Image Processing*. 2nd ed. San Diego, CA : Academic Press.

Shafiee, S., L. M. Lied, I. Burud, J. A. Dieseth, M. Alsheikh, and M. Lillemo. 2021. Sequential forward selection and support vector regression in comparison to LASSO regression for spring wheat yield prediction based on UAV imagery. *Computers and Electronics in Agriculture*, 183: 106036.

Shakoor, N., D. Northrup, S. Murray, and T. C. Mockler. 2019. Big Data Driven Agriculture: Big Data Analytics in Plant Breeding, Genomics, and the Use of Remote Sensing Technologies to Advance Crop Productivity. *The Plant Phenome Journal*, 2(1): 1-8.

Smith, G. M., and E. J. Milton. 1999. The use of the empirical line method to calibrate remotely sensed data to reflectance. *International Journal of Remote Sensing*, 20(13): 2653-2662.

Stow, D., C. J. Nichol, T. Wade, J. J. Assmann, G. Simpson, and C. Helfter. 2019. Illumination geometry and flying height influence surface reflectance and NDVI derived from multispectral UAS imagery. *Drones*, 3(3): 55.

Strecha, C., L. Van Gool, and P. Fua. 2008. A generative model for true orthorectification. In *Archives International Society for Photogrammetry and Remote Sensing*, 303-308. Beijing, China, July 3-11.

Taddia, Y., P. Russo, S. Lovo, and A. Pellegrinelli. 2020. Multispectral UAV monitoring of submerged seaweed in shallow water. *Applied Geomatics*, 12: 19-34.

Tattaris, M., M. P. Reynolds, and S. C. Chapman. 2016. A direct comparison of remote sensing approaches for high-throughput phenotyping in plant breeding. *Frontiers in Plant Science*, 7: 1131.

Togeirode Alckmin, G., A. Lucieer, R. Rawnsley, and L. Kooistra. 2022. Perennial ryegrass biomass retrieval through multispectral UAV data. *Computers and Electronics in Agriculture*, 193: 106574.

Valencia-Ortiz, M., W. Sangjan, M. G. Selvaraj, R. J. McGee, and S. Sankaran. 2021. Effect of the solar zenith angles at different latitudes on estimated crop vegetation indices. *Drones*, 5(3): 80.

Vermote, E., and J. C. Roger. 1996. Radiative transfer modelling for calibration and atmospheric correction. In *Advances in the Use of NOAA AVHRR Data for Land Applications*, eds. G. D'Souza, A. S. Belward, and J. P. Malingreau, ch. 3, 49-72. Dordrecht, The Netherlands : Kluwer Academic Publishers.

Wang, C., and S. W. Myint. 2015. A Simplified Empirical Line Method of Radiometric Calibration for Small Unmanned Aircraft Systems-Based Remote Sensing. *IEEE Journal of Selected Topics in Applied Earth Observations and Remote Sensing*, 8(5): 1876 - 1885.

Weiss, M., F. Jacob, and G. Duveiller. 2020. Remote sensing for agricultural applications: A meta-review. *Remote Sensing of Environment*, 236: 111402.

Wierzbicki, D., M. Kedzierski, A. Fryskowska, and J. Jasinski. 2018. Quality assessment of the bidirectional reflectance distribution function for NIR imagery Sequences from UAV. *Remote Sensing*, 10(9): 1348.

Xu, K., Y. Gong, S. Fang, K. Wang, Z. Lin, and F. Wang. 2019. Radiometric calibration of UAV remote sensing image with spectral angle constraint. *Remote Sensing*, 11(11): 1291.

Zhang, C., R. J. McGee, G. J. Vandemark, and S. Sankaran. 2021. Crop performance evaluation of chickpea and dry pea breeding lines across seasons and locations using phenomics data. *Frontiers in Plant Science*, 12: 604259.

Zhang, X., and D. H. Brainard. 2004. Estimation of saturated pixel values in digital color imaging. *Journal of the Optical Society of America A*, 21(12): 2301-2310.

Supplementary Materials

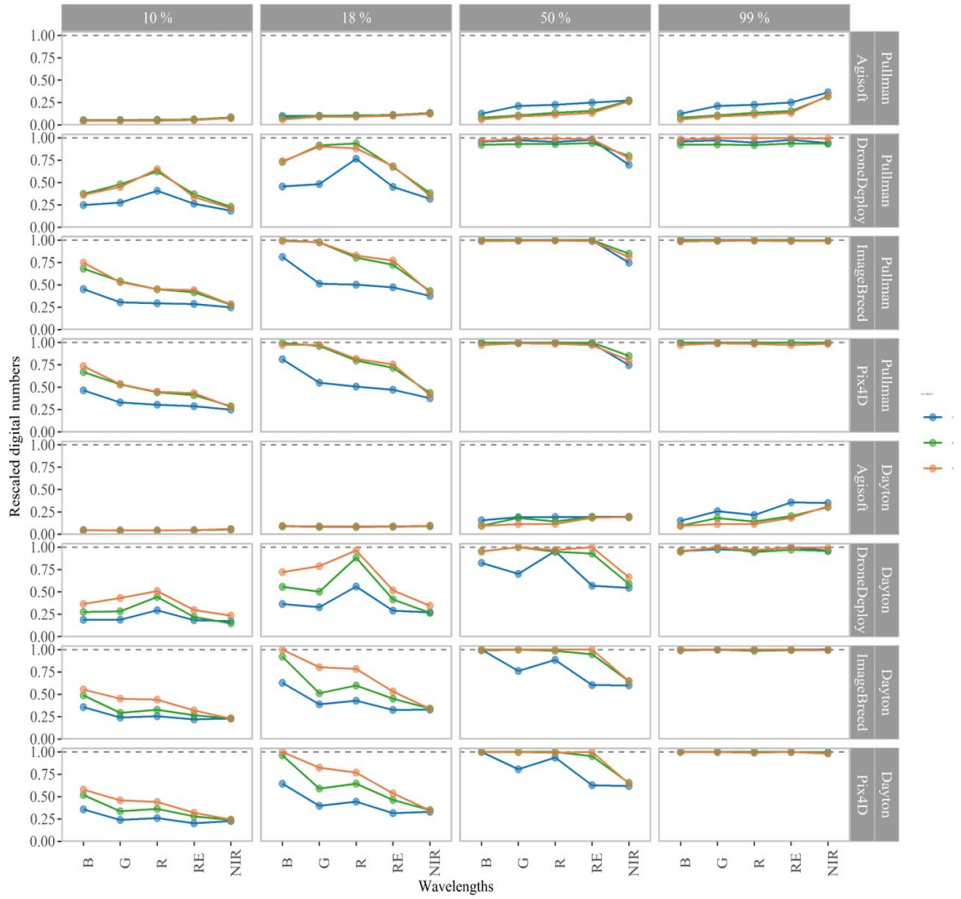

Figure S1 Rescaled digital number response from four reflectance panels (10%, 18%, 50%, and 99%), two locations (Pullman and Dayton), and four photogrammetric software (Agisoft, DroneDeploy, ImageBreed, and Pix4D).

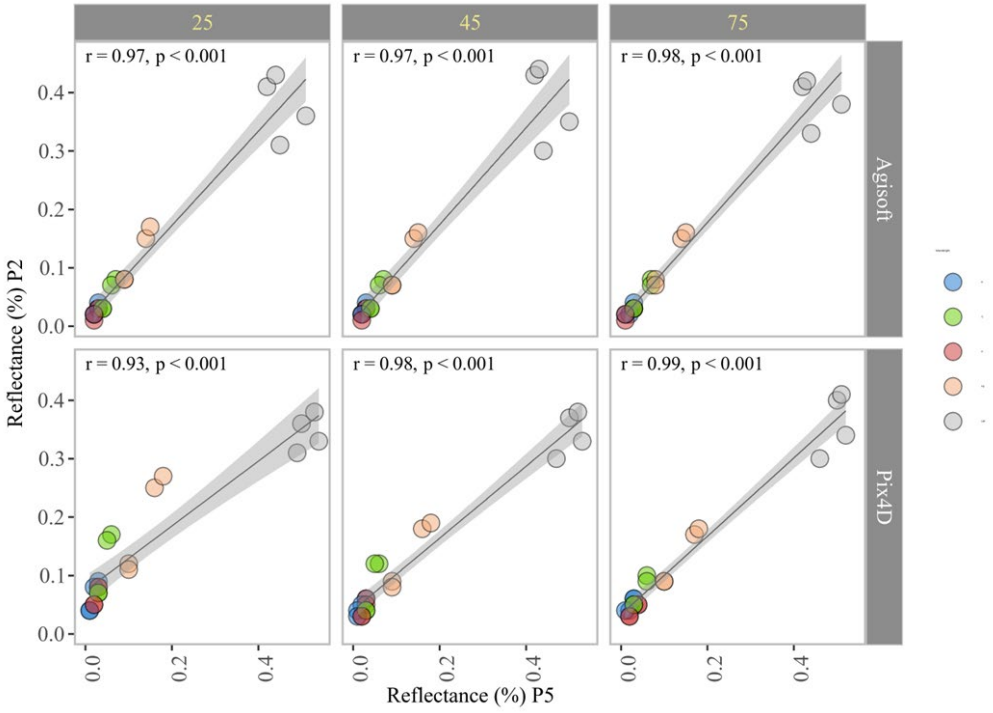

Figure S2 Crop reflectance correlation between panel of 18% (P2) and Micasense panel of 53% (P5) across altitudes and two photogrammetric software (Agisoft and Pix4D).

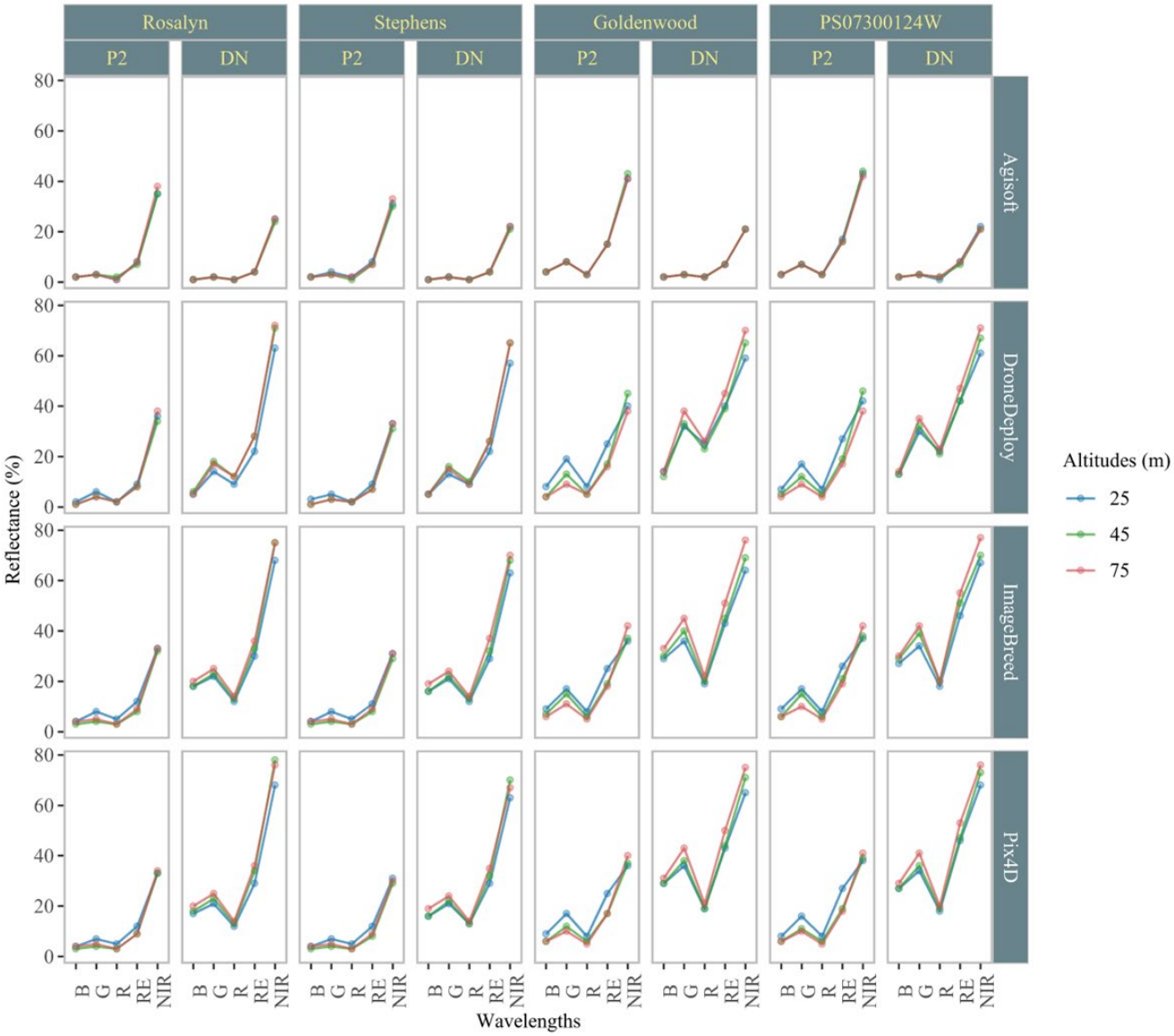

Figure S3 Spectral plant reflectance (radiometrically corrected with P2= 18%) and rescaled digital number across crop type, photogrammetric software, and flight altitudes. For this comparison, DN values were rescaled between 0 to 100.